

Superlattice Patterns in Vertically Oscillated Rayleigh-Bénard Convection

Jeffrey L. Rogers* and Michael F. Schatz†

Center for Nonlinear Science and School of Physics, Georgia Institute of Technology, Atlanta, Georgia 30332-0430

Oliver Brausch and Werner Pesch

Physikalisches Institut der Universität Bayreuth, Bayreuth, Germany 95440

(Received 28 June 2000)

We report the first observations of superlattices in thermal convection. The superlattices are selected by a four-mode resonance mechanism that is qualitatively different from the three-mode resonance responsible for complex-ordered patterns observed previously in other nonequilibrium systems. Numerical simulations quantitatively describe both the pattern structure and the stability boundaries of superlattices observed in laboratory experiments. In the presence of the inversion symmetry, superlattices are found numerically to bifurcate supercritically directly from conduction or from a striped base state.

PACS numbers: 47.54.+r, 05.45.-a, 47.20.Dr, 47.27.Te

Symmetry plays a crucial role in selecting the patterns displayed in physical, chemical, and biological systems as they are driven away from equilibrium [1]. Frequently, an initially homogeneous state loses stability with increasing driving to a regular pattern containing a narrow band of wave numbers. System symmetries select the allowable nonlinear mode interactions which dictate the pattern structure. In isotropic systems that are inversion symmetric (invariant under a change in sign of the field variables), periodic parallel stripes (rolls) or squares typically form at onset while hexagons form in the absence of inversion symmetry due to three-mode interactions (*resonant triads*). Under some conditions, *complex-ordered* [2] patterns displaying exotic spatial structure described by relatively few Fourier modes emerge at onset as the result of interactions between multiple disparate wave numbers. These exotic states include *superlattices*, which are spatially periodic, and *quasipatterns*, which have a definite rotational symmetry but are spatially aperiodic [3–5]. In all these cases, the lack of inversion symmetry allows resonant triads to determine the pattern structure [2–6].

We report the first experimental and numerical evidence of superlattices in Rayleigh-Bénard convection (RBC). Unlike previously observed complex-ordered patterns these superlattices may occur in the presence of inversion symmetry, which inhibits resonant triads. Instead, we find qualitatively different four-mode interactions (*resonant tetrads*) are responsible for selecting the patterns' planforms. One type of superlattice, which we call a square superlattice (SQS) [Fig. 1(a)], is found to bifurcate supercritically from conduction at a codimension-two (*bicritical*) point where linear modes of two disparate wave numbers simultaneously become marginally stable. Studies of RBC have helped reveal many basic principles in pattern formation since the experiments are precise and can often be directly compared with the theoretical description available through the Oberbeck-Boussinesq equations (OBE) [7]. Our results show that understanding of complex-ordered patterns in nonequilibrium systems

may be advanced by experimental/theoretical investigations of RBC.

Convection patterns with multiple distinct length and time scales are found in a thin fluid layer subjected both to a vertical thermal gradient and to vertical sinusoidal oscillations. Numerical predictions [8,9] recently confirmed by experiments [10] indicate such flows arise for sufficiently large Rayleigh number $R = \frac{\alpha g d^3 \Delta T}{\nu \kappa}$, with thermal expansivity α , gravitational acceleration g , fluid layer depth d , imposed temperature difference ΔT , kinematic viscosity ν , and thermal diffusivity κ . The critical Rayleigh number R_c depends on three additional parameters: Prandtl number $\text{Pr} = \frac{\nu}{\kappa}$, oscillation frequency $\omega = d^2 \omega' / \kappa$, and displacement amplitude $\delta = \frac{\kappa^2}{g d^4} \delta'$ (ω' and δ' are the dimensional frequency and amplitude, respectively). For fixed Pr and ω , modulated flows with a long-length scale and harmonic (H) temporal response (ω) arise for small δ . Short-length scale flows displaying subharmonic (S) temporal response ($\omega/2$) are found when δ is sufficiently large. At a bicritical point (δ_{2c}, R_{2c}), H and S modes arise simultaneously with distinct critical wave numbers q_{2c}^H and q_{2c}^S .

We study convection in thin layers of compressed CO_2 . The configuration of our experimental setup was described previously [10]. Results detailed in this Letter are obtained for $\text{Pr} = 0.930$ and $\omega = 98.0$ by quasistatically varying δ and R for a layer at a mean temperature of 34.00 ± 0.01 °C and pressure of 32.700 ± 0.001 bar. The layer depth is $d = 0.0650$ cm, yielding a characteristic vertical diffusion time $\frac{d^2}{\kappa} \approx 2$ sec. For these conditions, the bicritical point occurs at $\delta_{2c} = 3.768 \times 10^{-4}$, $R_{2c} = 4554$ with wave numbers $q_{2c}^H = 1.742$ and $q_{2c}^S = 5.173$ (scaled by d^{-1}). We also solve the OBE using a code tested for standard RBC [7,11], generalized to include time dependent acceleration [12]. Because of the applied pseudo-spectral method the spatial variations in the plane are naturally captured by 2D-Fourier modes. The simulations are typically performed on a 256×256 grid with periodic

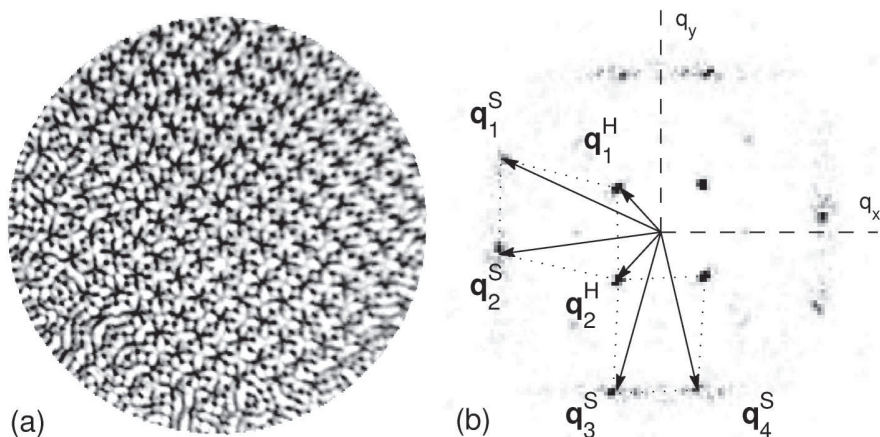


FIG. 1. Experimental SQS at $\delta = 3.58 \times 10^{-4}$ and $\epsilon_2 = 0.650$. These states display complex periodic spatial structure (a) and power spectra (b) typically dominated by twelve peaks with $|\mathbf{q}_i^H| \approx 0.95q_{2c}^H$ and $|\mathbf{q}_i^S| \approx 0.86q_{2c}^S$ for these parameter values.

boundary conditions and a time step $dt = 0.04(2\pi/\omega)$. We have further validated our numerical methods by reproducing known values of R_c and the associated critical wave numbers for both H and S onset, as well as typically observed experimental patterns. For presentation purposes we define a reduced Rayleigh number $\epsilon_2 = R/R_{2c} - 1$.

SQS display short-length scale, starlike structures located on a long-length scale square lattice [Fig. 1(a)]. The backbone square sublattice, which usually displays few defects in both experiments and simulations, is spanned by the H modes $\pm\mathbf{q}_1^H$ and $\pm\mathbf{q}_2^H$ with $|\mathbf{q}_i^H| \approx q_{2c}^H$ [Fig. 1(b)]. The starlike structures, which may have various orientations, are captured by the eight spectral peaks $\pm(\mathbf{q}_1^S, \mathbf{q}_2^S)$ and $\pm(\mathbf{q}_3^S, \mathbf{q}_4^S)$, where $|\mathbf{q}_i^S| \approx q_{2c}^S$; the peaks occur in pairs along lines parallel to sums and differences of $\pm\mathbf{q}_1^H$ and $\pm\mathbf{q}_2^H$. The end points of the wave vectors $\mathbf{q}_1^H, \mathbf{q}_2^H; \mathbf{q}_1^S, \mathbf{q}_2^S$ and $-\mathbf{q}_1^H, \mathbf{q}_2^H; \mathbf{q}_3^S, \mathbf{q}_4^S$ span parallelograms separated by an angle of approximately 90° [dotted lines in Fig. 1(b)].

Experiments find SQS states are attracting for a wide range of parameters except in the vicinity of the bicritical point (Fig. 2). The range of stable SQS is found by slowly increasing or decreasing a single parameter (δ or ϵ_2). No hysteresis is observed in determining the SQS parameter boundary, and the SQS patterns form independent of the initial state. SQS are observed for a range of δ from $\epsilon_2 \approx 0.38$ up to the largest ϵ_2 experimentally accessible (≈ 1). Over the SQS region $|\mathbf{q}_i^H|$ remains relatively constant with values from $0.91q_{2c}^H$ to $0.94q_{2c}^H$ while $|\mathbf{q}_i^S|$ decreases monotonically with increasing ϵ_2 from $0.92q_{2c}^S$ at $\epsilon_2 \approx 0.38$ to $0.78q_{2c}^S$ at $\epsilon_2 \approx 0.96$. For $0.2 \lesssim \epsilon_2 \lesssim 0.38$ over a narrow range of δ , the uniform square H sublattice found in SQS is supplanted by a disordered sublattice containing domains of locally square, rhombic, and hexagonal symmetries (see Fig. 4 in [10]). For $\epsilon_2 < 0.38$, the H sublattice is composed increasingly of hexagons with decreasing ϵ_2 . For $\epsilon_2 \gtrsim 0.2$, the S component displays starlike structures, while close to bicriticality ($\delta \approx \delta_{2c}$ and $\epsilon_2 \lesssim 0.2$) the S component is simply patches of rolls superimposed on a nearly uniform H hexagonal sublattice. For δ slightly less than δ_{2c} experiments find uniform,

pure H hexagons at onset. We attribute the appearance of hexagons to non-Boussinesq effects which break the fluid layer inversion symmetry about the midplane (Boussinesq symmetry) and allow for three-mode interactions between the H modes [13].

Our numerical simulations confirm many of the experimental findings and, additionally, allow investigation of the behavior near bicriticality in the presence of inversion symmetry. For $\epsilon_2 \approx 0.4$, numerical SQS stability boundaries, which are computed using random initial conditions, are in good agreement with experiment (Fig. 2). In accord with experiments SQS always form by locking into resonant states with $|\mathbf{q}_i^H| \approx q_{2c}^H$ and $|\mathbf{q}_i^S| \approx q_{2c}^S$. With decreasing ϵ_2 the SQS are found over a smoothly narrowing range of δ about δ_{2c} (Fig. 2, inset). The disordered H sublattices observed in experiments for $0.2 \lesssim \epsilon_2 \lesssim 0.38$ are typically seen only as transients in the simulations.

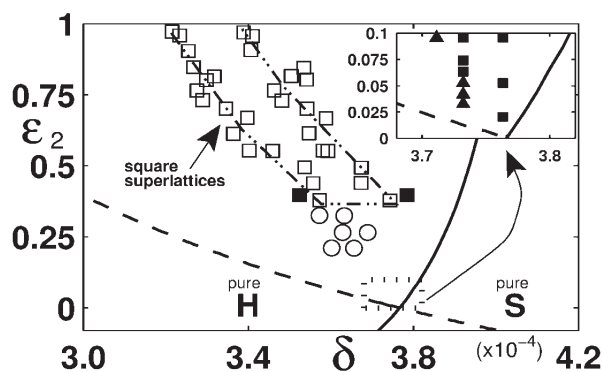


FIG. 2. Phase-plane showing the SQS stability boundaries as well as the codimension-two point at the intersection of the H (solid line) and S (dashed line) linear stability curves. Experimentally observed SQS boundary (\square) is reproduced in numerical solutions (\blacksquare) at $\epsilon_2 \approx 0.4$. Experimental patterns in the \circ bounded region display square, rhombic, and hexagonal symmetry in the H sublattice. Numerical results indicate SQS are the result of a supercritical primary bifurcation at the bicritical point (\blacksquare , inset). Simulations also find roll superlattices (\blacktriangle , inset), over a narrow parameter range, which bifurcate supercritically from H rolls.

Moving closer to the bicritical point the SQS patterns become more regular, i.e., the parallelograms in Fig. 1(b) become regular rectangles as $|\mathbf{q}_i^H| \rightarrow q_{2c}^H$ and $|\mathbf{q}_i^S| \rightarrow q_{2c}^S$. In this regime, obtaining SQS from random initial conditions becomes prohibitively difficult due to critical slowing down; thus, we used approximate SQS states with $\leq 10\%$ amplitude noise as initial conditions and found stable SQS patterns for ϵ_2 as small as 0.005. (For $\epsilon_2 < 0.005$ our grid in Fourier space has insufficient resolution to describe accurately the SQS mode structure.) At δ_{2c} we find the H and S mode amplitudes vary like $\sqrt{\epsilon_2}$, indicating the SQS bifurcate supercritically from conduction directly at the bicritical point.

Near the bicritical point, simulations find another superlattice state for $\delta \lesssim \delta_{2c}$. In this case, the conduction state becomes unstable to pure H rolls at onset. With increasing ϵ_2 a secondary instability leads to a state that we call *roll superlattices* [Fig. 3(b)]. They are (at least linearly) stable over a narrow parameter range before the transition to SQS at larger ϵ_2 . For instance, at $\delta = 3.732 \times 10^{-4}$ roll superlattices are observed for $0.033 \leq \epsilon_2 \leq 0.079$ (Fig. 2, inset). There exists partial bistability with SQS; for example, SQS can arise for $\epsilon_2 \geq 0.063$ at $\delta = 3.732 \times 10^{-4}$. Above the onset of roll superlattices the S mode amplitudes follow the common square-root law characteristic for a supercritical bifurcation.

The wave-vector structure of experimental and numerical superlattices indicate four-mode interactions are critical to superlattice formation. The parallelograms in q space [Fig. 1(b)] suggest the H and S modes in SQS patterns satisfy the resonance conditions

$$\begin{aligned} \pm(\mathbf{q}_1^H - \mathbf{q}_2^H) &= \pm(\mathbf{q}_1^S - \mathbf{q}_2^S); \\ \pm(\mathbf{q}_1^H + \mathbf{q}_2^H) &= \pm(\mathbf{q}_3^S - \mathbf{q}_4^S). \end{aligned} \quad (1)$$

Wave vectors for each mode class (H or S) need not be of equal magnitude to satisfy these relations; thus, Eq. (1) describes cases found in both experiments [Fig. 1(b)] and simulations where $|\mathbf{q}_i^S|$ may be different for each i when ϵ_2 is sufficiently large. A four-mode resonance also governs the roll superlattices. In this case, only three distinct spectral peaks are involved; these peaks form a parallelogram by the self-interaction of the H mode. The resonance condition takes the form $2\mathbf{q}_1^H = \mathbf{q}_1^S - \mathbf{q}_2^S$.

The noted prominence of the twelve modes in line with Eq. (1) suggests the SQS pattern may be represented using the ansatz of an eigenmode expansion in the spirit of a weakly nonlinear analysis. The pattern field $T(\mathbf{x}, t)$, which is the shadowgraph intensity or midplane temperature, may be defined as

$$\begin{aligned} T(\mathbf{x}, t) &= \text{Re} \left\{ V^H(t) \sum_{j=1}^2 A_j^H \exp(i\mathbf{q}_j^H \cdot \mathbf{x}) \right\} \\ &+ \text{Re} \left\{ V^S(t) \sum_{j=1}^4 A_j^S \exp(i\mathbf{q}_j^S \cdot \mathbf{x}) \right\}, \end{aligned} \quad (2)$$

where \mathbf{x} is the horizontal coordinate parallel to the plane of the fluid layer. The time dependence of the H and S

eigenmodes, $V^H(t)$ and $V^S(t)$, is given by Floquet's theorem: $V^{H,S} = \text{Re} \{ \exp(\mu^{H,S} t) \sum_{n=0}^{\infty} c_n^{H,S} \exp(in\omega t) \}$ (normalized to $|c_0^{H,S}| = 1$) with Floquet exponents $\mu^H = 0$ for H modes and $\mu^S = i\omega/2$ for S modes. The mode V^H is well described by retaining only the $n = 0$ and $n = 1$ terms; i.e., V^H is essentially sinusoidal with a constant offset (Fig. 4). By contrast, V^S contains several harmonics of $\omega/2$ satisfying the S time-translation symmetry $V^S(t + 2\pi/\omega) = -V^S(t)$. To represent the snapshot of a regular SQS [Fig. 3(a)], where the spectral peaks form rectangles, only two constant real amplitudes A and B with $A = A_1^H = -A_2^H$, $B = A_1^S = A_2^S = A_3^S = A_4^S$ are needed in Eq. (2). The amplitudes of the dominant Fourier modes in Eq. (2), which are directly available from the numerical temperature field, exhibit time dependence that is very well represented by $AV^H(t)$ and $BV^S(t)$ with adjusted amplitudes A, B (Fig. 4). The roll superlattice pattern [Fig. 3(b)] can be described analogously to Eq. (2) with one H amplitude A^H and two S amplitudes $A_{1,2}^S$, where $A_1^S = A_2^S = iB$.

The general structure of the cubic nonlinearities in the six coupled amplitude equations for SQS, which determine the six amplitudes A in Eq. (2), is suggested by four-wave resonance according to Eq. (1). Inversion symmetry rules out quadratic couplings. For the equation describing A_1^H at the cubic order, the common terms $\sim A_1^H |A_j^H|^2$ ($j = 1, 2$) and $\sim A_1^H |A_j^S|^2$ ($j = 1, \dots, 4$) exist with different coupling constants. However, according to Eq. (1) additional resonant coupling terms $\sim A_2^H A_1^S (A_2^S)^*$, $(A_2^H)^* A_3^S (A_4^S)^*$ play a crucial role. It should be noted that two phases for the four S amplitudes remain arbitrary within the amplitude equations up to cubic order. To fix them, higher order resonances, which are automatically included in the full OBE, come into play. The analogous coupled amplitude equations for the roll superlattice pattern contain a resonant coupling $\sim (A^H)^* A_1^S (A_2^S)^*$.

Superlattices in modulated thermal convection differ from superficially similar patterns observed in Faraday surface-wave [4] and optical [2,5] systems. First, although general theoretical insight into complex-ordered nonlinear patterns in the Faraday system has progressed impressively [14,15], we are not aware of quantitatively accurate comparisons with experiments. (The situation is similar in the

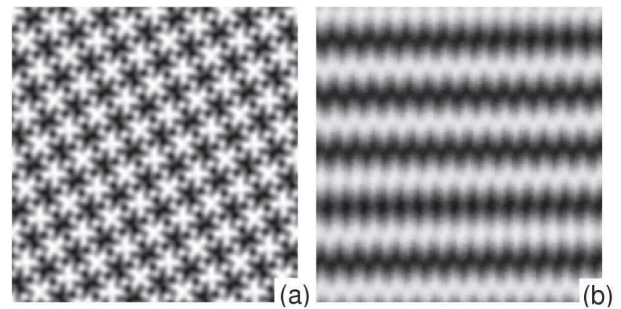


FIG. 3. Superlattices observed in numerics near the bicritical point: (a) SQS at $\delta = \delta_{2c}$ and $\epsilon_2 = 0.053$, (b) roll superlattice at $\delta = 3.732 \times 10^{-4}$ and $\epsilon_2 = 0.053$.

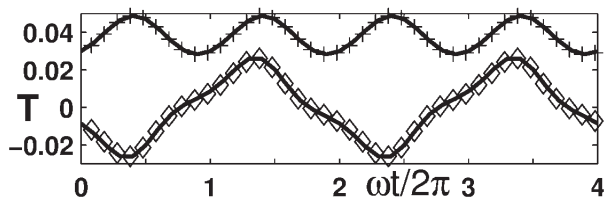


FIG. 4. The temporal variation of linear eigenvectors multiplied with adjusted amplitude factors $A = 0.0382$, $B = 0.0108$ (see text) at $\delta = 3.732 \times 10^{-4}$, $\epsilon_2 = 0.053$ for the H (upper curve) and S (lower curve) modes, respectively. Comparison is made with the numerical amplitudes of the Fourier modes at \mathbf{q}_1^H (+) and \mathbf{q}_1^S (\diamond), respectively, for the SQS midplane temperature field $T(\mathbf{x}, t)$ in units of ΔT .

optical case.) By contrast, superlattices observed in modulated RBC experiments can be quantitatively compared with solutions of the OBE. Second, while the temporal symmetry of invariance under discrete time translation by $2\pi/\omega$ rules out resonant triads among S modes in all parametrically modulated systems, resonant triads in Faraday waves are allowed by the interaction of S and H modes. In modulated Boussinesq RBC the additional symmetry of midplane inversion acts on both H and S modes; thus, all quadratic interactions are suppressed, and resonant tetrads are responsible for the formation of superlattices. Last, superlattices in the Faraday and optical systems must satisfy both frequency and wave number resonance conditions while those in modulated RBC need satisfy only a wave number condition. This can be understood by recalling that both Faraday waves (in the limit of small viscosity and infinite depth) and modulated RBC can be modeled by the Mathieu equation, which describes a vertically oscillated pendulum. The onset of surface waves in the Faraday case is analogous to the excitation of a hanging pendulum. (This also applies to the optics examples, where the waves are externally imposed.) However, onset in modulated RBC corresponds to the inverted pendulum [8], which has no natural frequencies about its (unstable) equilibrium.

This work suggests several directions for future investigations. We are currently investigating the effect of breaking inversion symmetry on pattern formation near the bicritical point by quantitatively comparing experiment and simulations that include non-Boussinesq effects. We expect other complex-ordered patterns may arise either by two-frequency driving, as suggested by recent results in Faraday experiments [3,4], or by using the sensitive dependence of q_{2c}^S on ω to vary the ratio q_{2c}^H/q_{2c}^S over the

experimentally accessible range of $1.7 \lesssim q_{2c}^H/q_{2c}^S \lesssim 5.5$. Finally, it is hoped this work will motivate mathematical investigations of resonant tetrad interactions involving equivariant perturbation theory [16] with the aim of rigorously characterizing new routes to complex-ordered patterns in nonequilibrium systems.

The authors thank Professor F. Busse, Professor L. Kramer, and Professor M. Silber for useful discussions. This work is supported by the NASA Office of Life and Microgravity Sciences Grant No. NAG3-2006.

*Electronic address: jeff@einstein.physics.gatech.edu

†Electronic address: mike.schatz@physics.gatech.edu

- [1] M. C. Cross and P. C. Hohenberg, *Rev. Mod. Phys.* **65**, 851 (1993).
- [2] L. M. Pismen and B. Y. Rubinstein, *Chaos Solitons Fractals* **10**, 761 (1999).
- [3] W. S. Edwards and S. Fauve, *Phys. Rev. E* **47**, R788 (1993); *J. Fluid Mech.* **278**, 123 (1994).
- [4] A. Kudrolli, B. Pier, and J. P. Gollub, *Physica (Amsterdam)* **123D**, 99 (1998); H. Arbell and J. Fineberg, *Phys. Rev. Lett.* **84**, 654 (2000); **81**, 4384 (1998); C. Wagner, H. W. Müller, and K. Knorr, *Phys. Rev. Lett.* **83**, 308 (1999).
- [5] J. B. Geddes, R. A. Indik, J. V. Moloney, and W. J. Firth, *Phys. Rev. A* **50**, 3471 (1994); E. Pampaloni, S. Residori, S. Soria, and F. T. Arecchi, *Phys. Rev. Lett.* **78**, 1042 (1997).
- [6] M. Silber and A. C. Skeldon, *Phys. Rev. E* **59**, 5446 (1999).
- [7] E. Bodenschatz, W. Pesch, and G. Ahlers, *Annu. Rev. Fluid Mech.* **32**, 709 (2000).
- [8] P. M. Gresho and R. L. Sani, *J. Fluid. Mech.* **40**, 783 (1970).
- [9] R. Clever, G. Schubert, and F. H. Busse, *Phys. Fluids A* **5**, 2430 (1993).
- [10] J. L. Rogers, M. F. Schatz, J. L. Bougie, and J. B. Swift, *Phys. Rev. Lett.* **84**, 87 (2000).
- [11] W. Pesch, *Chaos* **6**, 348 (1996).
- [12] Only minor modifications are required since the new oscillatory part of the buoyancy force (a linear term) is integrated explicitly in time by employing the approach used for quadratic nonlinearities described in [11].
- [13] F. H. Busse, *J. Fluid. Mech.* **30**, 625 (1967).
- [14] For a recent review see H. W. Müller, R. Friedrich, and D. Papathanassiou, in *Lectures Notes in Physics*, edited by F. Busse and S. C. Müller (Springer, New York, 1998).
- [15] W. Zhang and J. Viñals, *J. Fluid Mech.* **341**, 225 (1997).
- [16] S. L. Judd and M. Silber, *Physica (Amsterdam)* **136D**, 45 (2000).